Available online at www.sciencedirect.com

ScienceDirect

Physics Procedia 56 (2014) 610 – 619

Physics Procedia

8th International Conference on Photonic Technologies LANE 2014

Investigations on Laser Beam Welding Dissimilar Material Combinations of Austenitic High Manganese (FeMn) and Ferrite Steels

Velten Behm[a,b,*], Matthias Höfemann[d], Ansgar Hatscher[a], André Springer[c], Stefan Kaierle[c], David Hein[e], Manuel Otto[d], Ludger Overmeyer[c]

[a]*Volkswagen AG, Berliner Ring 2, 38440 Wolfsburg, Germany*
[b]*Sitech Sitztechnik GmbH, Stellfelder Straße 46, 38442 Wolfsburg, Germany*
[c]*Laser Zentrum Hannover e.V., Hollerithallee 8, 30419 Hannover, Germany*
[d]*Salzgitter Mannesmann Forschung GmbH, Einsenhüttenstraße 99, 38239 Salzgitter, Germany*
[e]*Laboratorium für Werkstoff- und Fügetechnik der Universität Paderborn, Pohlweg 47-49, 33098 Paderborn, Germany*

Abstract

For the past few years the customer's demand for more fuel efficient and at the same time safer vehicles has steadily increased. Consequently, light weight design has become one of the main interests in engineering.
With regard to sheet metal components, a new class of high manganese steels, based on the TWIP (twinning induced plasticity) effect, provides the opportunity of shaping light weight designed thin and complex sheet metal geometries with advanced crash performance.
In terms of weldability, due to their thermo-physical properties (high content of C, Mn, Al, Si), FeMn steels have to be handled differently in comparison to conventional steel grades. Particularly dissimilar material combinations of FeMn and ferrite steels are in the center of interest for industrial applications. This study reveals that metallurgical properties of dissimilar welding seams can be influenced considerably by laser beam welding, resulting in a change of the mechanical properties of the seam which is practicable without using filler material as described in (Flügge et al., 2011).

© 2014 Published by Elsevier B.V. This is an open access article under the CC BY-NC-ND license (http://creativecommons.org/licenses/by-nc-nd/3.0/).
Peer-review under responsibility of the Bayerisches Laserzentrum GmbH

Keywords: laser beam welding; dissimilar material combinations; FeMn; TWIP

* Corresponding author. Tel.: +49-5361-9993590 .
E-mail address: velten.behm@volkswagen.de

1875-3892 © 2014 Published by Elsevier B.V. This is an open access article under the CC BY-NC-ND license (http://creativecommons.org/licenses/by-nc-nd/3.0/).
Peer-review under responsibility of the Bayerisches Laserzentrum GmbH
doi:10.1016/j.phpro.2014.08.049

1. Introduction

As the automotive market is highly competitive, all stakeholders from supplying industry to OEM continuously need to provide new and innovative products to their customers. Additionally increasing legal requirements concerning for instance safety and environmental issues have to be satisfied in order to stay competitive.

An example for increasing environmental regulations is the limitation of CO_2 emissions for new cars, on which the European Union has placed a limit of a maximum of 95 g CO_2/km from the year 2020 on (European Union, 2009). Likewise 93 g CO_2/km are targeted in the USA from 2025 on (Eder, 2013).

In order to meet these partially contrary interests of customers and regulations, many companies have identified light weight design as one of the key disciplines for automotive development and success. With regard to sheet metal design a new class of high strength and ductile FeMn steels, based on the twinning induced plasticity effect (TWIP), offers promising properties for structural parts.

1.1. Mechanical properties of FeMn steels

The motivation for implementing FeMn steels into automotive production is their remarkable mechanical properties, which allow shaping of both light and good crash performance structural parts.

Compared to conventional steel grades, FeMn steels offer high strength as well as high ductility. In numbers this means that tensile strengths (TS) greater than 900 MPa and total elongations up to 60 % are characteristic values for non-work-hardened products (see Fig. 1 (a)). These special attributes can be used to design lighter and more complex metal components compared to other high strength steels. Furthermore, these parts still show a remarkable ductility reserve after forming, so that they can absorb a higher amount of crash energy.

1.2. Weldability of FeMn steels

In contrast to conventional sheet metal steels, FeMn steels contain a relatively high amount of carbon (< 1.6 wt.-%), manganese (< 35 wt.-%), aluminum (< 7.0 wt.-%) and silicon (< 4.0 wt.-%) (Gigacher, 2004). Due to their metallurgy, many of these steels maintain their one-phase austenitic crystal lattice after forming and heat treatment. In addition the austenitic phase leads to low heat conductivity and high a thermal expansion coefficient of FeMn alloys (see Table 1) which may cause hot cracks (Keil et al., 2011) in the weld metal and distortion of the workpiece after welding (Pries et al., 2011). This is the main reason why welding techniques with a low energy input are favorable to other welding techniques. In this context, laser beam welding offers the possibility to weld seams

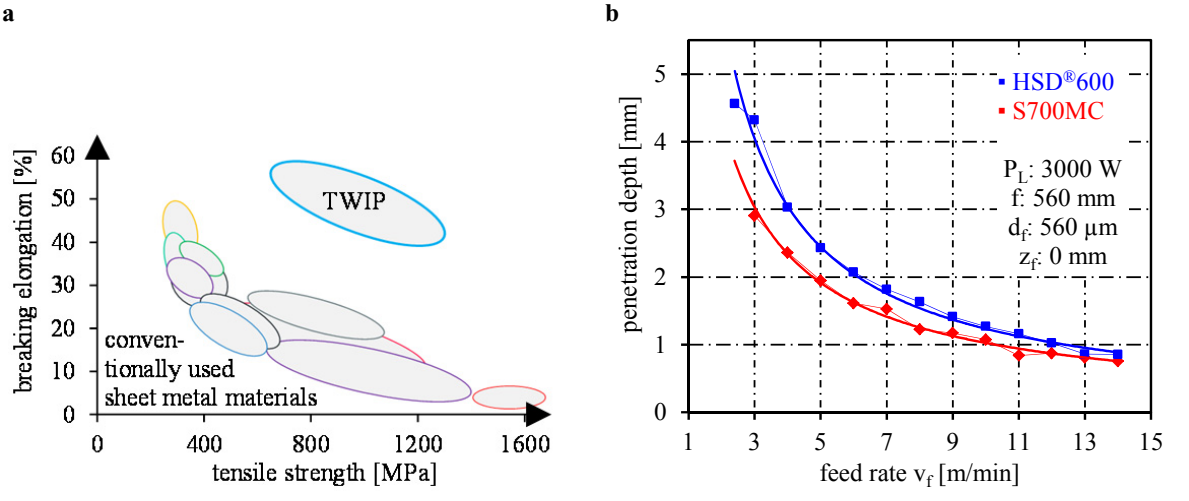

Fig. 1. (a) bubble chart: breaking elongation / tensile strength (Otto, 2011); (b) penetration depth of laser seams into a FeMn steel (HSD®600) compared to a low carbon steel (S700MC) (Behm et al., 2013).

having a narrow and deep shape, high feed rates, and minimum heat influence into the workpiece. Due to the low heat conductivity of FeMn steels, welding speeds can even be increased, in order to attain the same penetration depth as in low alloyed steels (see Fig. 1 (b)). This fact makes laser beam welding of FeMn steels more efficient than welding conventional steel grades.

Table 1. Thermo-physical properties of a selected alloys (Behm et al., 2013).

Alloy	Heat Conductivity [W/Km] at RT	Thermal Expansion Coefficient [10^{-6} K^{-1}]
Low Carbon Steel	45 - 55	13.6
Austenitic Stainless Steel (X5CrNi18-10)	15	16
FeMn / TWIP	< 12	> 21

Nomenclature

BPP	beam parameter product
d_f	fiber diameter
d_s	spot diameter
f	focal length of focusing lens
f_c	collimator: focal length
P_L	laser output power used
P_{Lmax}	maximum available laser output power
RT	room temperature
wt.-%	weight percent
z_f	focus plane : + = above workpiece's surface; - = underneath workpiece's surface
λ	wavelength

2. Experimental setup

This chapter includes the description of the experimental setup used for the investigations on laser welding of dissimilar material combinations of FeMn and ferrite steels.

2.1. Laser, optics and handling system

The experimental welding equipment consists of a disc laser with a maximum output power of 16,000 W (4000 W in use for experiments), an optical fiber of 200 µm in diameter, a collimator having a focal length of 200 mm and a focusing lens with a focal length of 560 mm. These components were chosen in order to match beam characteristics to those being widely used in automotive production lines (d_f ~ 600 µm).

In order to achieve the highest welding accuracy possible, and thus to obtain high repeatability of the welding experiments, a 3-axis CNC gantry system was used for handling laser optics and workpieces. In the following table, the main data of the experimental equipment and the process parameters are listed.

Table 2. Laser system used for experiments

	laser					optics			handling	
model designation	type*	λ* [nm]	BPP* [mm*mrad]	P_{Lmax}*/ P_L [W]	d_f [µm]	f_c [mm]	f [mm]	d_s [µm]	type	z_f [mm]
Trumpf Trudisk 16002	Yb:YAG	1030	8	16000/ 4000	200	200	560	~600	3-axis CNC	0

*source: Trumpf TruDisk 16002 data sheet

2.2. "KS-2" specimen

The KS-2 specimen was developed at the "Laboratory for Materials and Joining Technology" (LWF) in Paderborn, Germany (Hahn, 1995; Hahn 2004) and consists of two U-shaped profiles (see Fig. 2 (a)) joined together in an overlap configuration (DVS-EFB 3480-1, 2007). It is suitable for determining mechanical characteristics of quasi punctual joint elements under quasi-static, cyclic and impact loads.

One of the main advantages of the KS-2 specimen, compared to a conventional single overlap shear specimen is, that load directions can be varied stepwise from angles of 0° (shear load) to 90° (normal cross tension load) (see Fig. 2 (c)). In the present study, load conditions of 0°, 45° and 90° were investigated to determine characteristics of linear laser welded seams. Each of these seams was centered longitudinally on the specimen and had a length of 25 mm (see Fig. 2 (b)).

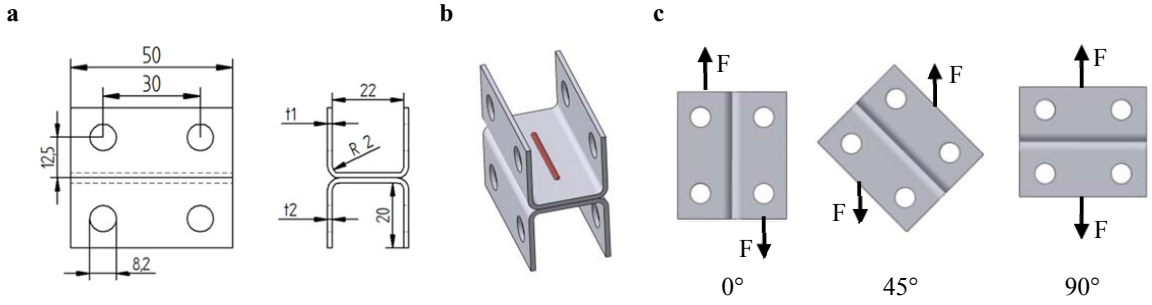

Fig. 2. (a) geometry of KS-2-specimen; (b) KS-2-specimen with laser seam of 25 mm; (c) load directions.

2.3. Description of test devices

In order to identify the behavior of laser welded seams produced with different laser parameters under varying load cases and load directions, adapted test devices had to be used for quasi-static and cyclic loads.

Quasi-static tests were carried out with at least five specimens per load direction (0°, 45° and 90°) and a testing

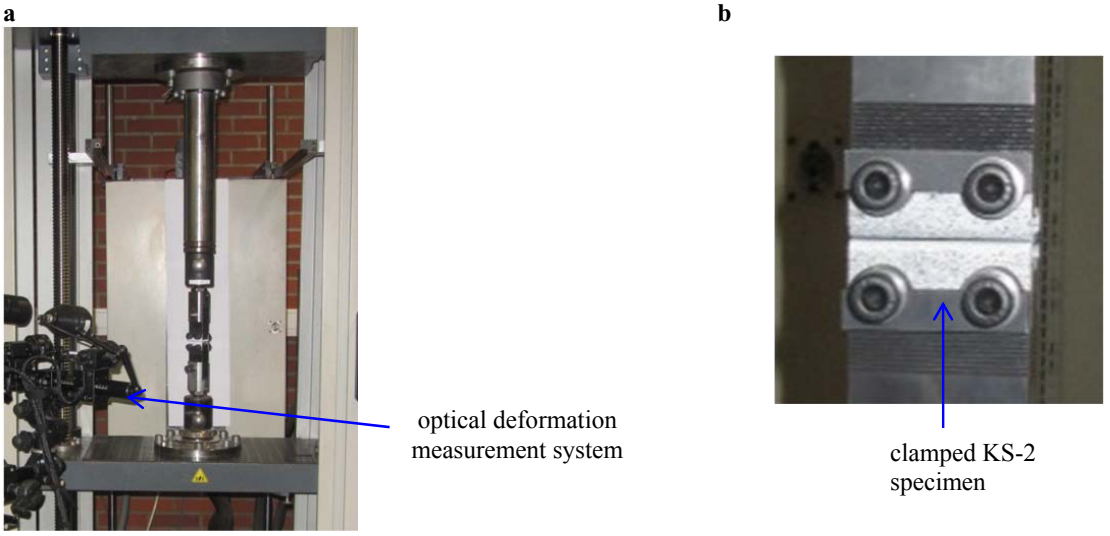

Fig. 3. Experimental setup for KS-2 tests (a) quasi-static tension test, (b) clamping device.

velocity of 10 mm/min. KS-2 specimens were mounted within special pivoting clamping jaws (see Fig. 3 (b)), which in turn were connected to an all-round tensile test device "Zwick/Roell Z100" (see Fig. 3 (a)).

In order to record applied forces during tensile testing, a piezoelectric load transducer with a nominal force of 100 kN was used.

Deformation was plotted in two manners. Firstly by recording the crosshead displacement (global deformation) and additionally by using an optical deformation measurement system (local deformation), called "GOM ARAMIS". For recording the specimens' "real" (local) deformations, an optical measurement system was used for more precise displacement, plots compared to crosshead's displacement also depending on the stiffness of the whole testing device.

Cyclic tensile shear tests were performed using a "Rumul" high frequency resonance pulse testing machine. The testing frequency was set to f = 70 Hz, and the R factor ($R = F_{c\text{-}min}/F_{c\text{-}max}$) was defined to be R = 0.1. In order to keep the number of tests within reasonable limits, a number of $N = 2\times10^6$ cycles was chosen to represent the fatigue life of the specimens. For these experiments, KS2-specimens were used under shear load (0°).

2.4. Material

All experiments were carried out with non-coated alloys. They include a FeMn alloy supplied by Salzgitter Flachstahl GmbH, called HSD®600 produced on a laboratory route, and two reference steels: a high strength HCT980X dual-phase-steel and a low alloyed S400MC. All metal sheets had a thickness of t = 1.5 mm. Table 3 lists the chemical composition as well as the mechanical properties of the test materials.

Table 3. Chemical composition and mechanical properties of sheet metal test materials

alloy	sheet thickness [mm]	chemical composition					mechanical properties		
		C [wt. %]	Mn [wt. %]	Al [wt. %]	Si [wt. %]	Cr [wt. %]	BE [A_{80} %]	YS [MPa]	TS [MPa]
HSD®600	1.5	0.7	15	2.5	2.5	-	52	600	1020
HCT980X*	1.5	0.15	1.5	0.04	0.5	-	11	810	1000
S420MC	1.5	0.035	0.6	0.04	0.02	0.13	17	420	540

*source: SSAB Docol® data sheet

3. Experiments and discussion

All welds were made using the equipment listed in Table 2. For welding, the laser output power was set to 4000 W. By means of overlap shear specimens experiments have shown that welding direction plays a major role in joining dissimilar material combinations of FeMn and ferrite steels. Welding from FeMn steel (upper sheet) to low carbon steel (lower sheet) generally results in higher joint strength and reliability (Behm et al. 2013). For this reason, all dissimilar material combinations were processed in the same way in this study – FeMn steel on top and low carbon steel underneath.

In order to minimize the complexity of the technical equipment of the welding tool, no filler material was used. Therefore the chemical composition and the mixing ratio can only be changed by varying penetration depth. Fig. 4 shows the evolution of mixing ratio in dependence on penetration depth, respectively welding speed. By means of the etchant "Klemm-I" bright and dark colored areas of the weld metal can be visualized. Bright colored weld metal corresponds to a hardness of ~ 270 $HV_{0.5}$, and dark colored weld metal corresponds to hardness of up to 600 $HV_{0.5}$ (Behm et al., 2013). The appearance of martensitic structure in the dissimilar weld seams considered can result from the concentration shift between FeMn and low carbon steels (compare Table 3). While welding, alloying elements of FeMn steels are continuously mixed with those of the low carbon steel. Consequently the concentration of austenite and ferrite formers within the weld metal changes compared to the base metal. According to the mixing ratio and the weld pool dynamics, some areas in the seam are rich in austenite formers, and thus are able to stabilize an austenitic phase. Other areas are not able to stabilize the austenitic phase, and due to self-quenching effects combined with increased carbon content, martensitic structures are formed in these parts of the seam.

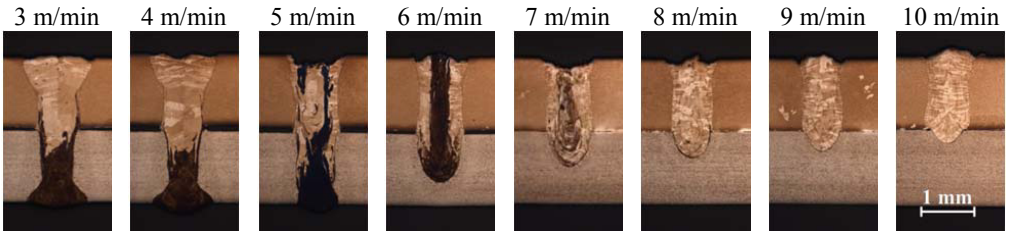

Fig. 4. Evolution of mixing ratio of HSD®600 1,5 mm (top) and S420MC 1,5 mm (bottom) in dependence of penetration depth / welding speed.

As shown in Fig. 4, full penetration seams (see Fig. 4 - 3 and 4 m/min) result in a weld metal distribution dividable into a lower martensitic area and an upper austenitic area. The border between both structures is situated in large parts within the lower joining member (S420MC), so that the joining plane widely consists of an austenitic structure. Only some thin fingerlike martensitic areas spread vertically upwards. Due to the weld pool dynamics, these vertical martensitic "fingers" are situated in the outer weld metal and may reach the seam plane level.

As soon as the energy per unit length is reduced, and no stable through weld can be ensured, weld pool dynamics change in a way that the vertical mixture between the upper (FeMn) and lower (low carbon steel increases) joining partners increases (see Fig. 4 - 5 m/min). The result is an irregular distribution between martensitic and austenitic structure within the whole seam.

Further reduction of the penetration depth stabilizes weld pool dynamics again, leading to a characteristic metallographic appearance of the weld metal (see Fig. 4 - 6 m/min): Martensitic phase (column) in the middle and the bottom of the seam bordered by austenite phases on the right and left hand side. Even though weld pool dynamics remain basically the same, the aforementioned sharp distinction regresses with a permanent decrease of penetration depth (see Fig. 4 - 7 – 10 m/min). That is because the amount of austenite forming elements within the weld pool relatively increases, and creation of martensitic structure is more and more suppressed.

In order to evaluate the influence of the austenitic and martensitic structure on the mechanical properties of the weld metal three types of seams were chosen. Firstly a trough welded (see Fig. 4 - 3 m/min) joint. Secondly a partial penetration weld containing considerable amounts of martensitic as well as austenitic structure (see Fig. 4 - 6 m/min). And finally an almost martensite free (martensitic structure in transition area to ferrite steel) seam was chosen, which still had a reliable penetration depth and joint width (see Fig. 4 - 8 m/min).

3.1. Quasi-static tension tests

The aim of quasi-static tension tests was to identify the influence of martensitic structure on mechanical properties of laser welded dissimilar material combinations between FeMn and ferrite steel seams under different load directions. In order to realize load directions of 0°, 45° and 90°, tests were carried out as described in chapter 2 using KS-2 specimens.

By processing dissimilar metal joints with feed rates of 3 m/min, 6 m/min and 8 m/min (see Fig. 4), different penetration depths and weld pool dynamics were realized, leading to different weld metal mixing ratios and martensitic structure distributions. As a reference, through welded similar material combinations (feed rate 3 m/min) of FeMn (HSD®600), low carbon steel (S420MC) and dual-phase steel (HCT980X) were tested. By way of illustration, Fig. 5 shows on the left hand side exemplary force/displacement plots of individual specimens consisting of all six tested material combinations. On the right hand side, bar charts display values for maximum force (F_{max}) and maximum local displacement (DISP) at F_{max}, which were averaged over all tensile tests. All tensile tested specimens of all material combinations broke along the weld metal, and none has pulled out. Comparing maximum average forces (F_{max}) and maximum average displacements (DISP) of all similar and dissimilar laser welded material combinations for shear loads (0°) (see Fig. 5 (a)), it appears that the combination HCT980X→HCT980X supports the highest average forces, and the combination S420MC→S420MC shows the highest average displacements and thus ductility. The similar material combination of HSD®600 is situated in between both the aforementioned combinations concerning F_{max}, and ductility. In terms of F_{max} all three dissimilar

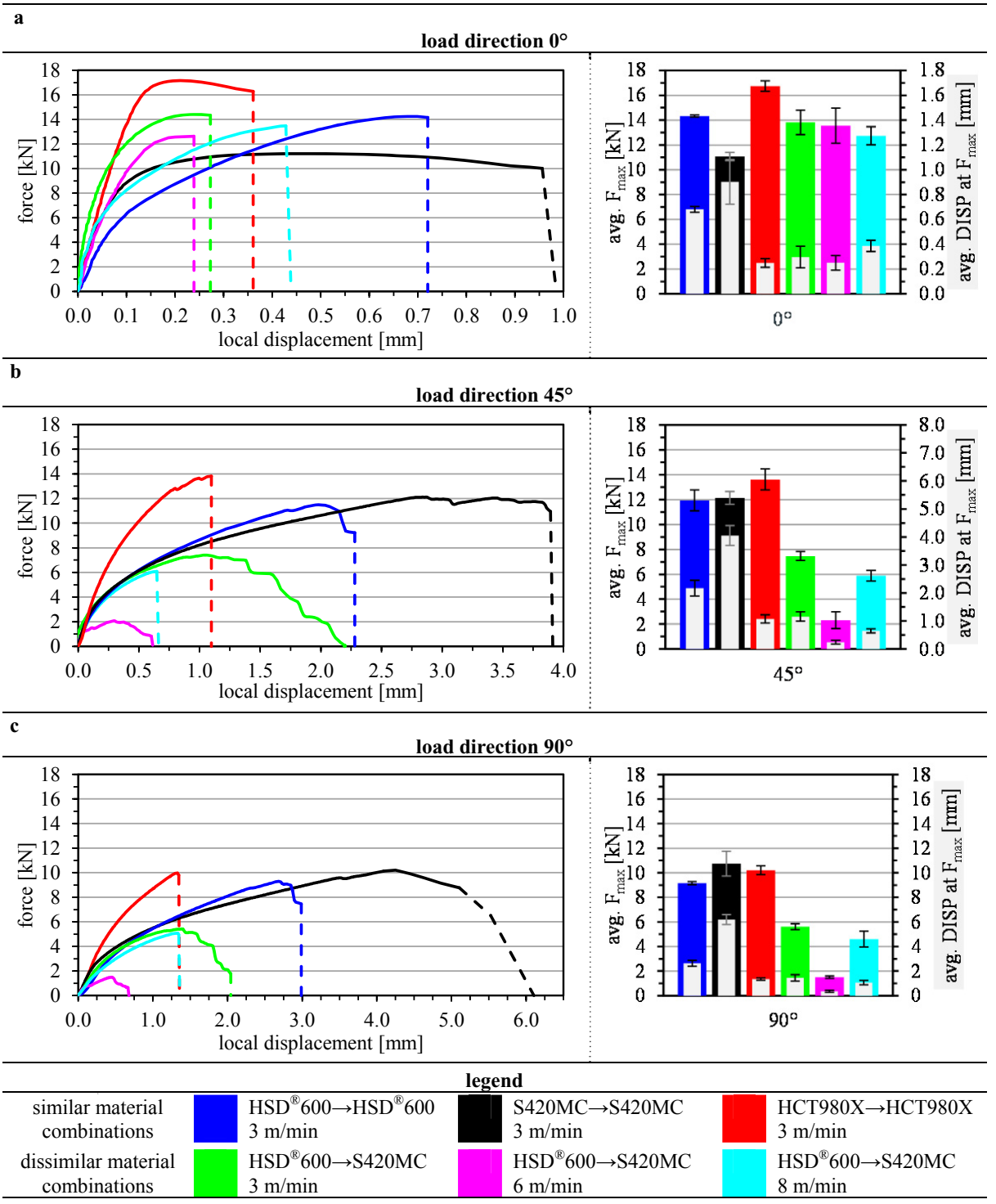

Fig. 5. Results of quasi-static tension tests of laser welded KS-2 specimens (25 mm step seam) in form of exemplary force/displacement plots (left) and bar charts (right) including averaged values for load directions of (a) 0°, (b) 45° and (c) 90°.

seams show comparable values to HSD®600→HSD®600 and higher values than the combination S420MC→S420MC. Comparing the dissimilar seams "3 m/min", "6 m/min" and "8 m/min" among themselves, it appears that the weld metal of austenitic structure (8 m/min) is the most ductile one, whereas a high content of martensitic structure within the joining plane (6 m/min) leads to lower average displacement values. With regard to F_{max}, the seam "3 m/min" shows the highest average values. On closer examination of Fig. 5 (b), displaying results of tension tests for load direction of 45° (50 % shear load, 50 % normal load), all joints where showed that the maximum force decreases, except for the combination S420MC→S420MC, which even shows a slight increase of F_{max} values. On the other hand, average displacements strongly increase, which can be led back to specimens' deformation due to the applied load normal of 45°. With focus on dissimilar material combinations and maximum force values, it appears that the seams "3 m/min" or "8 m/min" perform half as good as they did on shear load. With high amounts of martensitic structure within the weld seams (6 m/min) maximum forces decrease even more – to one third compared to the two other dissimilar material combinations examined, and to one sixth of the maximum force, reported for pure shear loads (0°).

Fig. 5 (c) shows a force/displacement plot and a bar chart for a normal load (90°). Comparing these graphs to Fig. 5 (b), it appears, that maximum supported forces decrease and displacement increases, whereas the bar chart displays a comparable distribution of these values. Again, the similar combination of S420MC→S420MC is the only one to remain F_{max} on a comparable level as for 0° and 45°. With regard to dissimilar material combinations, specimens processed with 6 m/min show the most brittle behavior. "3 m/min" specimens show the best performance in terms of force and displacement values even though "8 m/min" specimens do have mostly austenitic structure.

Quasi-static tension tests have revealed that similar and dissimilar material combinations show comparable maximum forces. As soon as normal loads are applied (45° and 90°), maximum forces decrease for similar as well for dissimilar material configurations including partly martensitic (HCT980X) or austenitic (HSD®600) weld structure, whereas ferrite combinations of S420MC→S420MC show stable F_{max} values for all load directions. It appears that not only the presence of martensitic structure within the weld metal influences brittle fracture behavior (i.e. 6 m/min), but also the distribution of these martensitic areas. For instance, both "3 m/min" and "6 m/min" specimens contain martensitic structure in the seam plane. Load directions of 45° and 90° "6 m/min" seams show the lowest; and for of "3 m/min" seams show the highest force and displacement values compared to the other dissimilar material combinations, albeit "8 m/min" seams are austenitic. Consequently, it is favorable to produce weld seams containing stiff fingerlike martensitic structure situated in the outer regions of the seam with a ductile austenitic center. Martensitic areas seem to stabilize the austenitic structure and counteract against crack initiation originating from the overlap joint notch.

3.2. Cyclic tests

Cyclic tests were carried out in order to evaluate the fatigue limit of dissimilar material combinations of FeMn and low carbon steels. They were performed using the described machine and specimens (see chapter 2). The results of the experiments are displayed in a graph of the logarithmic scale of a cyclic maximum force ($F_{c\text{-}max}$) against the logarithmic scale of cycles to failure (N) (see Fig. 6 (a)).

Fig. 6 (a) shows that similarly welded HSD®600 specimens have the highest fatigue resistance compared to the other examined material combinations. However, the curve of the martensitic structure containing "3 m/min" dissimilar material seams is situated lower, but close to the HSD®600→HSD®600 combination. In contrast to this result, the highest notch sensitivity can be attributed to the "6 m/min" weld seams, also including martensitic structure. The third dissimilar material combination (8 m/min), having a completely austenitic microstructure performs better and can be located in-between the aforementioned dissimilar material combinations. With regard to the ferrite weld seams (S420MC→S420MC) it can be noticed that these joints show a comparatively low performance.

The relatively good fatigue strength of the "3 m/min" specimens confirms what has been found out in quasi-static tensile tests. Consequently, the theory that the distribution of martensitic structure within the weld influences strongly the mechanical properties of the joint can also be transferred to cyclic loads. The martensitic structures in the outer regions of the weld reaching into the joining plane lead to lower notch sensitivity by counteracting against crack initiation and reinforcing the austenitic structure.

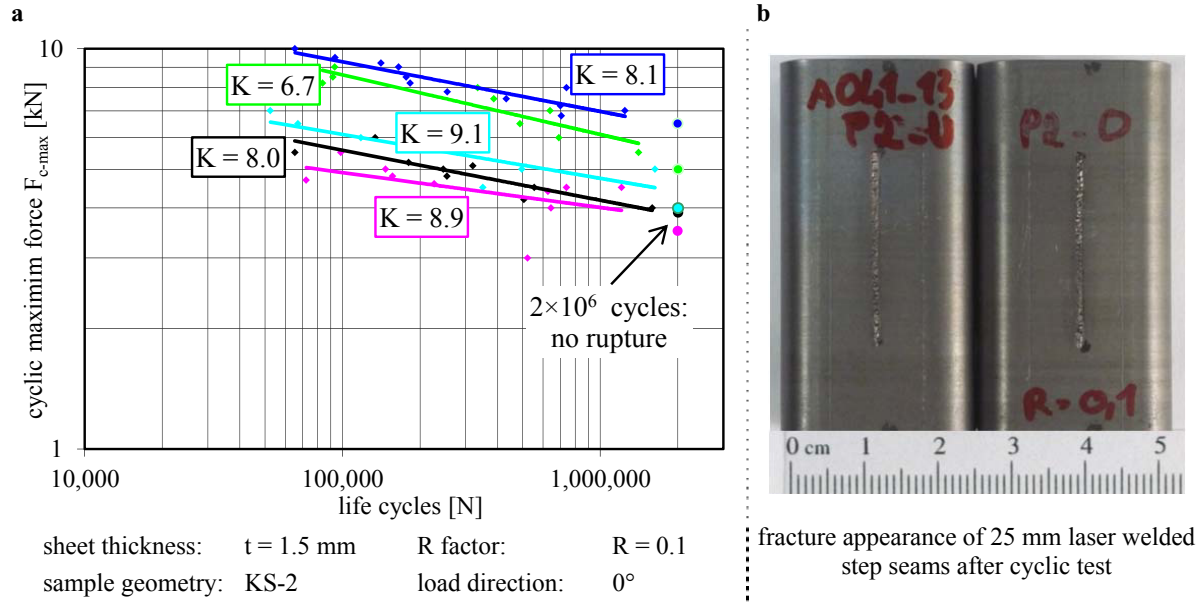

legend			
similar material combinations	HSD®600→HSD®600 3 m/min	S420MC→S420MC 3 m/min	
dissimilar material combinations	HSD®600→S420MC 3 m/min	HSD®600→S420MC 6 m/min	HSD®600→S420MC 8 m/min

Fig. 6. (a) Wöhler curves of different material combinations; (b) exemplary fracture appearance of similar welded HSD®600 after cyclic test.

In order to get a better idea of the typical fracture appearance of the specimens after cyclic tests, Fig. 6 (b) displays an example of fatigue fracture of the HSD®600→HSD®600 combination. In accordance with this appearance, all test series' specimens broke in the joining plane.

4. Conclusion

FeMn steels offer a high potential for light-weight construction. In order to take advantage of them in welded assemblies including conventional steels, it is important to identify process windows for creating process-reliable weld seams. Offering low heat input, laser welding has been assessed in this study for processing dissimilar material combinations. Without using a filler material, it has been shown that varying welding parameters lead to different weld metal compositions, hardness distributions and mechanical properties.

Experiments have shown that under different load directions, weld metal composition and distribution have an influence on joint strength, ductility and fatigue life.

This is especially true when changing hardness distributions within the joining plane are present. It was shown that martensitic structures, widely said to have negative effects on ductility and joint strengths, may also have a positive impact on exactly these values, when distributed the right way within the joining plane. In consequence laser welding offers the possibility to produce seams that, under certain conditions, show adequate mechanical properties, even without using filler material.

References

Behm, V., Huinink, S., Otto, M., Höfemann, M., Springer, A., Kaierle, S., 2013. Laser Welding of Fully Austenitic Twinning Induced Plasticity (TWIP) Steels, in: ICALEO 2013 Proceedings. 32nd International Congress on Applications of Lasers & Electro-Optics (ICALEO), Miami, FL. 05.-10.10.2013.

DVS-EFB 3480-1, 2007. Testing of properties of joints - Testing of properties of mechanical and hybrid (mechanical/bonded) joints. Beuth Verlag GmbH, Berlin, Heidelberg.

Eder, F., 2013. Deutsche Industrie fürchtet Aus für Premiumautos. http://www.welt.de/wirtschaft/article116392594/Deutsche-Industrie-fuerchtet-Aus-fuer-Premiumautos.html. Accessed 3 April 2014.

European Union, 2009. integrated approach to reduce CO2 emissions from light-duty vehicles: (EC) No 443/2009.

Flügge, W., Höfemann, M., Springub, B., Georgeou, Z., 2011. Schweißzusatz zum Lichtbogen- und Laserstrahlschweißen von Mischverbindungen aus austenitischem und ferritischem Stahl. patent application: DE102011121705A1.

Gigacher, G., 2004. Metallographische Besonderheiten bei hochmanganlegierten Stählen, Montanuniversität Leoben.

Hahn, O., 1995. Sample for testing of strength of spot welds or riveted joints. patent application: DE000019522247A1.

Hahn, O., 2004. Process for the preparation of samples and testing device. patent: DE000019522 247B4.

Keil, D., Zinke, M., Pries, H., 2011. Investigations on Hot Cracking of Novel High Manganese TWIP-Steels, in: Hot Cracking Phenomena in Welds III. Springer-Verlag Berlin Heidelberg, Berlin, Heidelberg, pp. 209–223.

Otto, M., 2011. HSD®-Stahl – optimierter TWIP-Stahl im Legierungssystem Fe-Mn-Al-Si, in: Werkstoffe im Automobilbau 2011. Innovative Werkstoffe für den Automobilbau I. Werkstoffe im Automobilbau 2011, Stuttgart. 23.05.2011. Springer Fachmedien Wiesbaden GmbH, Wiesbaden.

Pries, H., Zinke, M., 2011. Metallkundlich-technologische Untersuchungen zur Schweißeignung neuartiger austenitischer FeMn-Stähle. Final Report: DVS-Nr. 1.058. Deutscher Verband für Schweißen und verwandte Verfahren e.V., Düsseldorf.